Applied Catalysis B: Environmental 88 (2009) 323–330

Contents lists available at ScienceDirect

Applied Catalysis B: Environmental

journal homepage: www.elsevier.com/locate/apcatb

Immobilization of hydrothermally produced TiO_2 with different phase composition for photocatalytic degradation of phenol

Roberto Scotti [a,*], Massimiliano D'Arienzo [a], Franca Morazzoni [a], Ignazio Renato Bellobono [b]

[a] Department of Materials Science, INSTM, University of Milano-Bicocca, Via R.Cozzi 53, I-20125 Milano, Italy
[b] Department of Physical Chemistry, Environmental Research Center, University of Milano, Via Golgi 19, I-20133 Milano, Italy

ARTICLE INFO

Article history:
Received 4 September 2008
Received in revised form 24 October 2008
Accepted 2 November 2008
Available online 17 November 2008

Keywords:
Photocatalysis
Rutile
Anatase
Hydrothermal
Phenol mineralization

ABSTRACT

Hydrothermally produced TiO_2 powders with different phase composition (anatase, rutile and mixed phase) were immobilized on glass fibers and tested in the phenol mineralization process. Both H_2O_2 and O_2 were used as oxygen donors, and their performances were compared with those of the same TiO_2 samples as slurries.

The catalytic properties of the immobilized different crystalline phases, rutile and anatase, show the same trend as the slurry samples: pure rutile displays the highest catalytic efficiency in the presence of H_2O_2, while samples containing anatase improve the photodegradation efficacy with O_2. It was suggested that the stability of the photogenerated electron–hole couple allows high activity of rutile in the presence of H_2O_2, while the relevant oxygen chemisorption on anatase causes high catalytic activity in the presence of O_2. A four parameters kinetics model shows that both reaction steps, the phenol degradation and the mineralization of the intermediates, are photoactivated by TiO_2.

Photoactivity of the coated glass fibers is generally lower than that of slurries, even if their efficiencies are almost comparable when the oxidation is performed by H_2O_2, while much lower when the oxygen donor is O_2. As a matter of fact, the morphology of immobilized catalysts shows the presence of chestnut burr aggregates of large rutile crystalline rods on the glass fiber, which are much less compact than the aggregates of small anatase particles. This preserves rutile surface area from the coarsening effects; thus, when rutile is the more active species, as in the presence of H_2O_2, the photocatalytic activity is less affected by immobilization.

1. Introduction

Recent literature reports about several attempts to immobilize TiO_2 powder on different supporting materials [1–21], when titania is used as photocatalyst for the degradation of hazardous organic compounds in air or water. In fact the simple use of powder catalyst, especially in the nanosized form, has the disadvantage of a difficult sedimentation after the photocatalytic process; in addition TiO_2 nanoparticles, dispersed in the surrounding, may be hazardous, due to their potential inflammatory and cytotoxic effects [22].

TiO_2 was generally supported on SiO_2 glass beads [1], rings [2], and reactor tubular walls [3,4]; fiber-glass [5,6]; quartz [7,8]; zeolites [9,10]; perlite [11]; pumice [12]; alumina-based ceramic [13]; stainless steel [14,15]; aluminum [16]; polymeric membranes [17–19], etc. Recently natural fibers began to be used as suitable supports and the cotton material was conveniently adapted inside the photoreactors [20,21].

In spite of the different TiO_2 crystalline phases (anatase, rutile and brookite), most of the literature on immobilized catalysts is focused on the use of commercial P25 photocatalyst or of anatase, due to the small average size of the particles (<50 nm); in fact it is expected that the smaller the particle size the higher the surface area suitable for the catalytic activity. No attention, until lately, was directed to the possibility that other properties beside the surface area, like crystal shape and the oxygen source, could be influent.

Very recently we demonstrated that the catalytic activity of TiO_2 in the degradation of phenol (PhOH) in water depends on both the average particle size and the type of oxygen donor (O_2 or H_2O_2). Specifically, when the oxygen donor was H_2O_2, the large crystals of pure rutile or rutile-rich mixtures showed the highest activity; oppositely, when using O_2, anatase and anatase-rich mixtures are the most active [23,24]. This behavior was attributed to the slow recombination rate of the electron–hole couple in rutile large nanocrystals, which controls the catalytic mechanism when the

* Corresponding author. Tel.: +39 02 64485123; fax: +39 02 64485400.
E-mail address: Roberto.Scotti@unimib.it (R. Scotti).

0926-3373/$ – see front matter © 2008 Elsevier B.V. All rights reserved.
doi:10.1016/j.apcatb.2008.11.012

oxidant is H_2O_2. On the contrary, the easy oxygen chemisorption at the surface of the small anatase particles controls the mechanism when the oxygen donor is O_2.

The present paper reports about the immobilization on glass fibers, of a number of hydrothermal titania samples with different phase composition and, as a consequence, with different average particle size. Catalysts were characterized both as pure and supported powders. The catalytic activity of the samples as slurry was compared with that of the immobilized ones in the PhOH degradation reaction, using both H_2O_2 and O_2. The aim was to investigate how much the immobilization process affects the catalytic activity, and to verify whether the trend of the catalytic activity observed in slurry samples keeps the same in supported samples.

2. Experimental

2.1. Synthesis of TiO_2 and immobilization on glass fibers

Nanocrystalline TiO_2 was obtained by hydrothermal synthesis according to the previously reported procedure [23] by reacting aqueous solutions of $TiOCl_2$ (Aldrich, 99%) and NH_3 (Fluka, >25 wt%) in a teflon lined autoclave (Parr, model 4768Q). The autoclave was heated at 2.67 °C/min to a temperature of 30 °C below the set up temperature and then at 0.75 °C/min up to 220 °C.

The suspension was aged for 2 h at this temperature. The autoclave was then cooled in air outside the oven until the temperature dropped below 70 °C. After decantation, TiO_2 powder was recovered from the autoclave and washed first with water, then with ammonia solution and finally with acetone. Titanium dioxide nanoparticles were recovered by filtration and dried under vacuum at room temperature. The phase composition was determined by X-ray diffraction (XRD) patterns (see Section 2.2).

TiO_2 samples with different phase composition, labeled as Rnn, where nn represents the weight% of rutile phase (Table 1) were selected for the immobilization on glass fiber (glass fiber filter Whatman GF/A). TiO_2 powder (1.0 g) was suspended by sonication in 13.2 mL of water. While stirring, polyethylene glycol (PEG 2000) aqueous solution (5.0 g, 50 wt%) and few drops of Triton X-100 were added sequentially in order to obtain the suitable viscosity for a good and uniform coating adhesion. The mixture was homogeneously pasted on the glass fiber material (size 7 cm × 20 cm) with a brush and left to dry in an oven at 120 °C for 30 min. Successively, the coating was calcined at 400 °C in air for 30 min to fully remove the organic content. The final amount of TiO_2 deposited on glass fiber was 5.5 ± 0.5 g cm^{-2}. Finally, such immobilized photocatalyst was inserted into the reactor for the photocatalytic tests.

Hereafter, TiO_2 coated glass fiber were labeled as Rnn (i), where nn stand for the weight% of rutile phase and (i) indicates the immobilization on the fiber.

Table 1
Phase composition, BET specific surface area and XRD particle size of hydrothermal TiO_2 powder samples.

	Crystal phase composition		BET surface area (m^2 g^{-1})	XRD particle size (nm)	
	Anatase (wt%)	Rutile (wt%)		Anatase d(1 0 1)	Rutile d(1 1 0)
R100	0	100	20	–	58
R70	30	70	46	14	68
R57	43	57	64	15	31
R0	100	0	91	15	–

2.2. TiO_2 characterization

The X-ray diffraction patterns of the TiO_2 powders, collected with a Bruker D8 Advance diffractometer (Cu Kα radiation) operating in the range 20–40° 2θ (2θ step 0.020°, counting time 2 s per step), were used to determine the crystalline phase and the average crystallite size.

The diffraction peaks were indexed as pure rutile TiO_2 (JCPDS, no. 21-1276), and pure anatase (JCPDS, no. 21-1272). The phase contents were estimated using the following equation [25]:

$$f_A = \frac{1}{(1 + 1/KI_R/I_A)} \quad (1)$$

where f_A is the fraction of the anatase phase in the powder; $K = 0.79$ when $f_A > 0.2$ and $K = 0.68$ when $f_A < 0.2$; I_R and I_A are the integrated intensities of the rutile 1 1 0 and anatase 1 0 1 peaks, respectively.

The average crystallite size of TiO_2 was estimated from the broadening of the XRD peaks 1 1 0 for rutile and 1 0 1 for anatase by means of the Scherrer equation.

TiO_2 powder specific surface area (BET method) was determined by nitrogen physisorption (Micromeritics, ASAP 2010), after evacuation at 200 °C for 12 h.

Scanning electron microscopy (SEM) measurements were performed by a LEO 1450VP instrument both on powders and on supported catalysts.

High-resolution transmission electron microscopy (HRTEM) and electron diffraction (ED) were performed using a Jeol 3010 apparatus operated at 300 kV with a high-resolution pole piece (0.17 nm point-to-point resolution) and equipped with a Gatan slow-scan 794 CCD camera. The powders were suspended in isopropanol, and a 5 μL drop of this suspension was deposited on a holey carbon film supported on 3-mm copper grid for TEM investigation.

2.3. Photocatalytic experiments

Photodegradation experiments were carried out in a 600 mL discontinuous batch reactor with an external cooling jacket, and equipped with a UV 125 W Hg high-pressure lamp, placed in a coaxial quartz cylinder. No optical filter was adopted. The scheme of the photocatalytic apparatus is reported in Fig. 1. The experiments were performed using both TiO_2 coated glass fibers and TiO_2 slurries as catalysts in water.

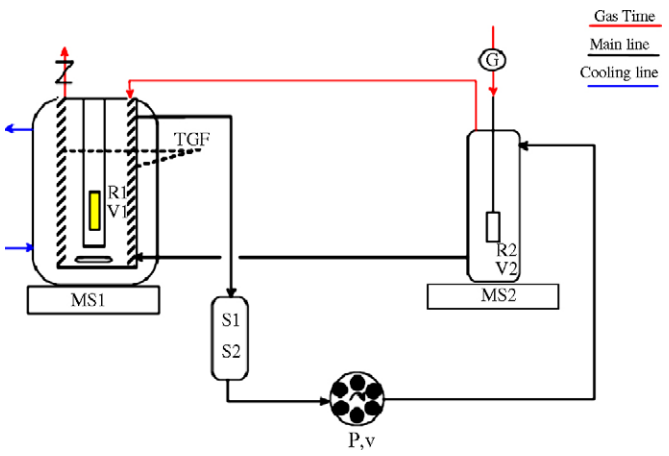

Fig. 1. Scheme of the photocatalytic apparatus used for the catalytic test. R1: photoreactor (volume, V1); R2: saturator (volume, V2); P: peristaltic pump (volumetric flux, v); S1, S2: sensors (pH, DO: dissolved oxygen); MS1, MS2: magnetic stirrers; G: gas flow meter; TGF: TiO_2 coated glass fiber.

In the former case the glass fiber was placed inside the batch reactor, sticked to the inner cylindrical walls at 4 cm from the coaxial UV lamp. PhOH solution (600 mL containing 121 ± 2 mg L^{-1} of PhOH, 93 ± 2 mg L^{-1} as *C*) was recirculated by a peristaltic pump with a speed of 14 mL s^{-1}. The temperature was kept 25 ± 2 °C; pH and dissolved oxygen content of the suspension were monitored by on-line sensors. In the case of the slurry, TiO_2 powder (150 ± 5 mg; 0.25 g L^{-1}) was suspended by sonication in 600 mL of water containing the same concentration of PhOH and recirculated with the same speed and at the same temperature as in the experiments on immobilized samples. It was verified that the catalyst loading in the range 0.2–1.4 g L^{-1} does not affect the kinetics parameters of PhOH mineralization.

Photodegradation was performed by using H_2O_2 or O_2 as oxygen donors, and operating either with slurries or with

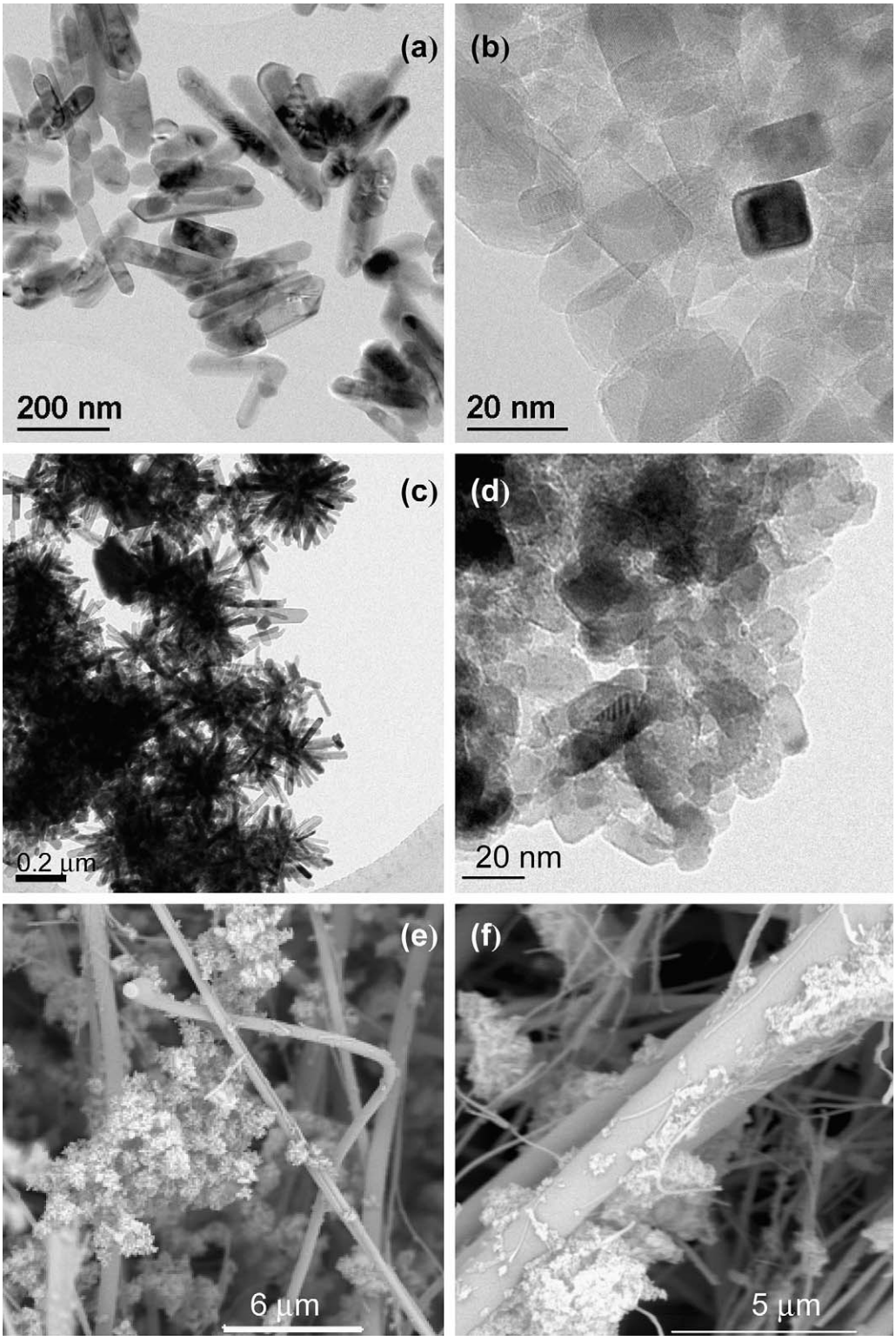

Fig. 2. TEM micrograph of (a) R100 and (b) R0 hydrothermal powders; (c) R100 and (d) R0 hydrothermal powders annealed at 400 °C in air; SEM micrographs (HV = 15.2 kV) of (e) R100 (i) (magnification 26.67k×) and (f) R0 (i) (magnification 19.67k×) coated glass fibers.

immobilized samples of photocatalysts, in order to compare the different experimental procedures. In the experiments performed with H_2O_2 (partly heterogeneous oxidation), stoichiometric amounts of aqueous H_2O_2 (35 wt%) were added (H_2O_2/PhOH = 14 - mol/mol) and the suspensions or the solutions, when using the immobilized photocatalysts, were circulated in the dark for 30 min before turning on the UV source. When the oxidations were carried out in the presence of O_2, and in the absence of any H_2O_2 (entirely heterogeneous oxidation), the suspensions or the solutions were circulated in the dark and saturated in an on-line chamber by continuously bubbling oxygen (100 mL min^{-1}); the excess of gas was eliminated through the non-return check valve. The UV source was turned on when the oxygen content in the suspension became maximum and constant (in about 10 min). The reaction was performed by keeping the oxygen feed constant. In both cases reference experiments were carried out in the absence of TiO_2 (blank), as well as by using commercial Degussa P25 titanium dioxide as photocatalyst. The kinetics of photoinduced PhOH degradation was monitored until the complete mineralization of the substrate, by withdrawing suspension aliquots (6 mL) of the reaction solution at regular intervals and analyzing them for the total organic carbon (TOC) by a Shimadzu TOC-V CSH analyzer. In the case of the slurry, TiO_2 powder was separated by centrifugation before TOC analysis.

3. Results and discussion

3.1. Morphological characterization of catalysts

TEM micrographs of R100 and R0 powders are reported in Fig. 2(a) and (b), respectively. Rutile particles show elongated shape with a width of about 60 nm and an aspect ratio α (α = length/width) of about 5. Anatase particles are small and almost cubic (5–15 nm) with α = 1–3.

Sizes and shapes of rutile and anatase crystals in mixed phase samples (not shown in figure) reflect those observed in the corresponding pure phases. The average crystal size calculated from the broadening of XRD 1 0 1 anatase peak (Table 1) is in agreement with TEM results. As the rutile crystals grow along the *c*-axis, the particle size calculated from the broadening of XRD 1 1 0 peaks corresponds to the width of the crystal.

After further annealing in air at 400 °C, the temperature of glass fiber calcination, both R100 and R0 powders undergo aggregation. R100 forms chestnut burr aggregates of rutile prismatic rods (Fig. 2(c)), while R0 more compact aggregates of square ended anatase nanoparticles (Fig. 2(d)).

SEM micrographs of TiO_2 coated glass fibers R100 (i) and R0 (i) show the presence of immobilized aggregates (Fig. 2(e) and (f)) whose morphology is reminiscent of that observed in the corresponding powders.

3.2. Photocatalytic activity

The photooxidation mechanism, as suggested by several authors [26,27], implies that electron–hole pairs are generated into TiO_2 by supra-band gap UV irradiation.

Free holes (h^+) are trapped by the organic molecule on the surface, giving direct photogeneration of organic radicals:

$$PhOH + h^+ \rightarrow PhO^\bullet + H^+ \quad (2)$$

alternatively they are fixed to terminal lattice oxide ions giving O^- and $^\bullet OH$ radicals:

$$O^{2-} + h^+ \rightarrow O^- \quad (3)$$

$$O^{2-} + h^+ + H^+ \rightarrow {}^\bullet OH \quad (4)$$

O^- and $^\bullet OH$ species react with the organic substrates, generating the corresponding radicals [28]:

$$O^-/{}^\bullet OH + PhOH \rightarrow O^{2-}/OH^- + PhO^\bullet + H^+ \quad (5)$$

which are further oxidized to other intermediates [29–31] until complete mineralization to CO_2 and H_2O.

Photogenerated conduction band electrons (e^-) may interact with the oxidant (H_2O_2 or O_2) according to the following reactions [26,27,32,33]:

$$H_2O_2 + e^- \rightarrow {}^\bullet OH + OH^- \quad (6)$$

$$O_2 + e^- \rightarrow O_2^{\bullet -} \quad (7)$$

where $O_2^{\bullet -}$ may further generate H_2O_2:

$$O_2^{\bullet -} + H_2O \rightarrow HO_2^\bullet + OH^- \quad (8)$$

$$HO_2^\bullet + H_2O + e^- \rightarrow H_2O_2 + OH^- \quad (9)$$

$$H_2O_2 + O_2^{\bullet -} \rightarrow {}^\bullet OH + OH^- + O_2 \quad (10)$$

and successively, $^\bullet OH$ radicals via reaction (5).

Besides, when using H_2O_2, direct photolysis of peroxide may also produce hydroxyl radicals [34,35]:

$$H_2O_2 \xrightarrow{h\nu} 2{}^\bullet OH \quad (11)$$

The photocatalytic activity of TiO_2 with different phase composition (Table 1) either immobilized on glass fiber as slurry in water, was measured in the PhOH mineralization, using H_2O_2 or

Table 2
Photocatalytic parameters of slurry and glass fiber immobilized TiO_2 samples.

Samples	Rutile fraction (wt%)	Photocatalytic parameters			
		H_2O_2		O_2	
		$(dC/dt)_{max}$ (mg L^{-1} min^{-1})	$t_{1/2}$ (min)	$(dC/dt)_{max}$ (mg L^{-1} min^{-1})	$t_{1/2}$ (min)
R100	100	2.00	38	0.155	349
R70	70	2.09	38	0.379	153
R57	57	1.61	50	0.457	134
R0	0	0.84	80	0.459	128
P25	20	1.50	55	0.682	95
Blank	–	1.27	74	0.075	740
R100 (i)	100	1.82	50	0.065	658
R70 (i)	70	1.36	54	0.058	639
R57 (i)	57	1.27	55	0.192	399
R0 (i)	0	1.21	70	0.210	472
P25 (i)	20	0.98	62	0.220	524

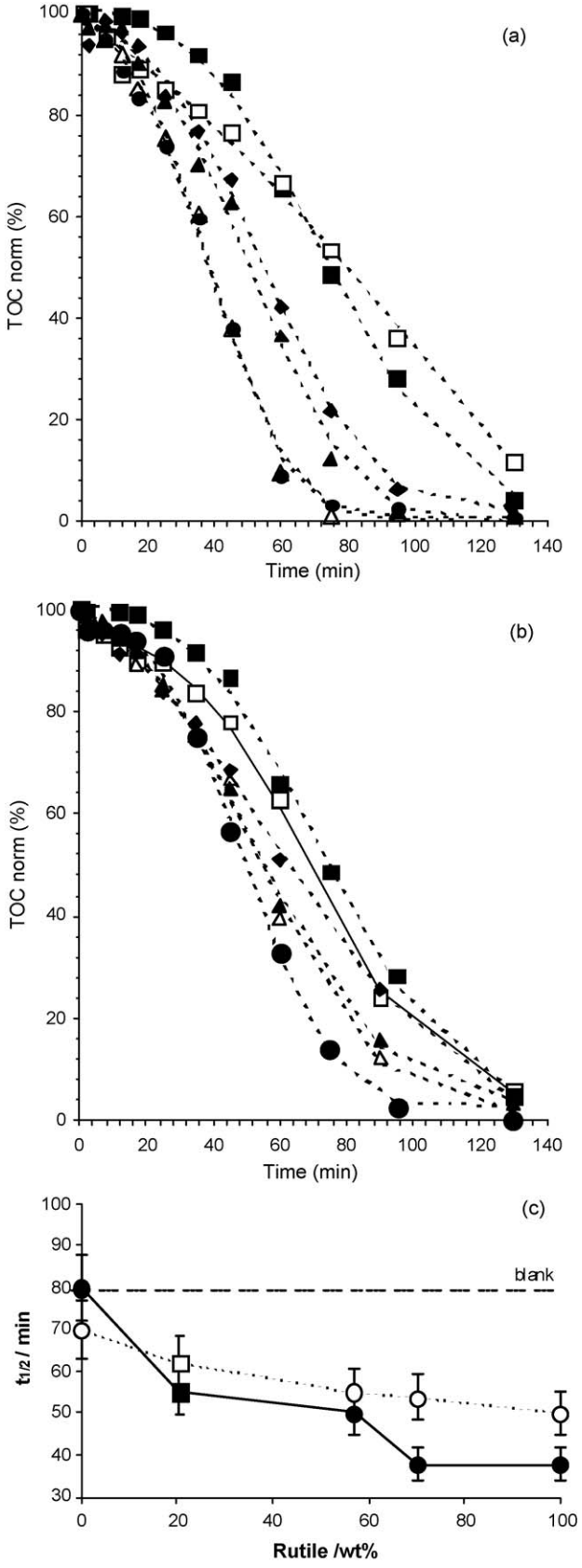

Fig. 3. Mineralization curves of phenol (given as TOC%) in the presence of the catalysts (a) in slurry and (b) immobilized on glass fiber using H_2O_2 as oxygen donor: (■) blank; (□) R0; (Δ) R70; (▲)R57; (●) R100; (◆) P25. Dashed lines are the best fit to the experimental data according to Eq. (12). (c) Half transformation time ($t_{1/2}$) of TOC against rutile fraction (wt%) for hydrothermal powder (●,○) and P25 (■, □) samples in the slurry (full dots) and immobilized on glass fiber (empty dots). 100% TOC at $t = 0$ corresponds to phenol amount before UV irradiation.

O_2 as oxygen donors under UV irradiation. The catalyst activity was evaluated by reproducing the experimental data (TOC vs. time) with the function

$$C(t) = C_0 - A\int_0^x \exp\left(-\frac{(t-t_0)^2}{s}\right)dt \quad (12)$$

where $C(t)$ is the TOC amount measured at the t time and C_0, A, t_0, s are fitting parameters (C_0 is the total organic carbon in solution after 30 min in the dark before the photocatalytic PhOH degradation and t_0 the time at which the mineralization of the organic substrate starts). The maximum degradation rate $(dC/dt)_{max}$, which corresponds to the maximum slope point of the fitted curves, and the half degradation time $t_{1/2}$, were taken as representative parameters of the kinetic behavior of the different samples. Both $(dC/dt)_{max}$ and $t_{1/2}$ values were calculated from Eq. (12) after optimization of the fitting parameters and were normalized to the same mass (150 mg) of TiO_2.

In all the performed experiments, during the initial phase of recirculation in the dark (30 min), the loaded PhOH concentration decreased of about 5.0 ± 1.5% in presence of both H_2O_2 or O_2 oxygen donors.

The experimental data related to TOC disappearance and the fitted curves of PhOH mineralization in the presence of H_2O_2, for both TiO_2 coated glass fiber and slurry, are reported in Table 2 and Fig. 3(a) and (b), where 100% TOC at $t = 0$ is the PhOH concentration measured just before switching on UV irradiation.

The trend is similar for both types of samples: $t_{1/2}$ value decreases and $(dC/dt)_{max}$ increases by increasing the rutile content and/or the particle size, as already widely discussed in analogous photocatalytic experiments [23,24]. The highest photocatalytic activity was observed for pure rutile, R100, having large prismatic crystals with high aspect ratio α, while pure anatase, R0, exhibits the lowest activity, of the same order than the blank test performed in the absence of TiO_2. These results confirm the relevance of the crystalline rutile nanorods in increasing the photocatalytic activity. Well-crystallized and well faceted nanocrystals involve relatively low concentration of defects, both in the bulk and on the surface, avoiding recombination of the photoexcited electron–hole pairs [36–38].

Accordingly the photoactivity of immobilized TiO_2 when using H_2O_2 as oxidant is only slightly lower than that of TiO_2 powder oxidized as a slurry (Fig. 3(c)).

If the PhOH mineralization was performed in the presence of O_2 as oxygen donor, the photocatalytic activity is generally lower than in the case of H_2O_2. Besides the photoactivity of TiO_2 coated glass fiber is significantly lower than that of TiO_2 powder in the slurry.

Also in this case, however, the photoactivity trend is similar for both immobilized and slurry samples (Fig. 4(a) and (b)): the values of $t_{1/2}$ decrease and those of $(dC/dt)_{max}$ increase with the increase of the anatase amount (Table 2). Pure rutile shows the lowest photoactivity. These results confirm that the presence of anatase is essential to improve the photocatalytic activity when O_2 is the oxygen donor [24] and that small differences exist between pure anatase and mixed phase samples. The higher photoactivity of anatase in the presence of O_2 can be related to its high ability to chemisorb O_2 as O_2^-; this extends the independent lifetime of electrons and holes, decreasing the $e^- – h^+$ recombination rate also in small particles [24].

In the blank, without the catalyst, the PhOH mineralization rate is very low, thus indicating a minor and negligible contribution of direct PhOH photolysis to the overall process.

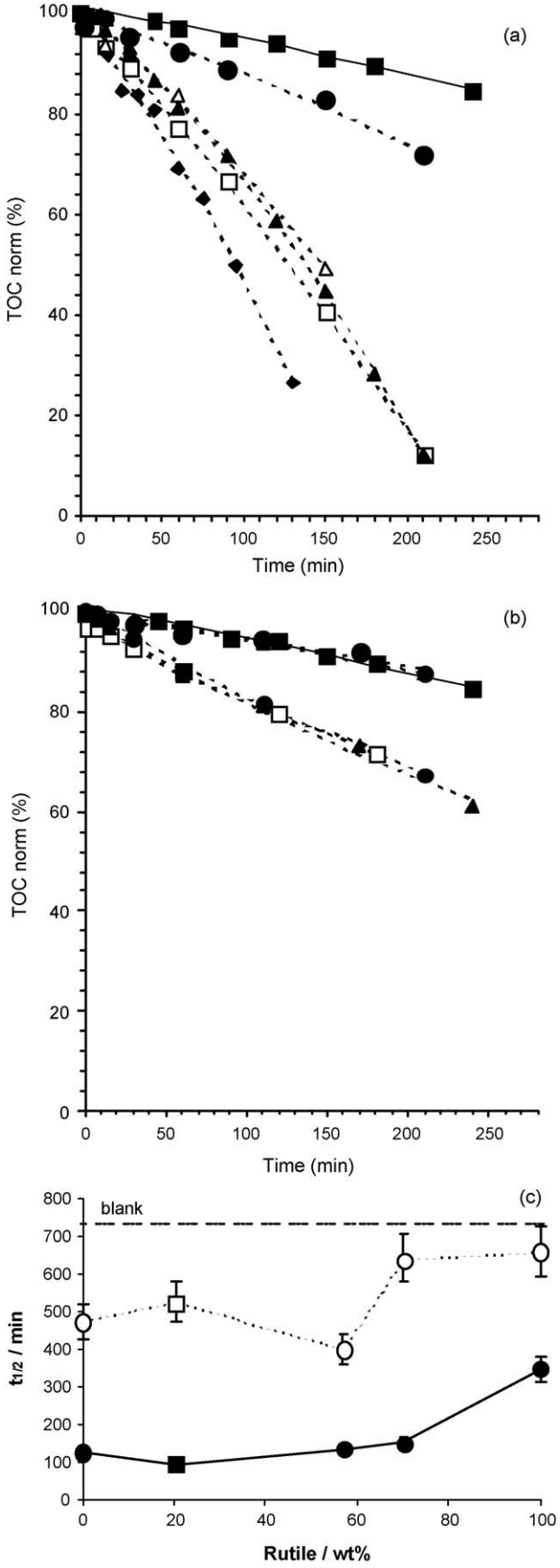

Fig. 4. Mineralization curves of phenol (given as TOC%) in the presence of the catalysts (a) in slurry and (b) immobilized on glass fiber using O_2 as oxygen donor: (■) blank; (□) R0; (Δ) R70; (▲)R57; (●) R100; (◆) P25. Dashed lines are the best fit to the experimental data according to Eq. (12). (c) Half transformation time ($t_{1/2}$) of TOC against rutile fraction (wt%) for hydrothermal powder (●,○) and P25 (■, □) samples in the slurry (full dots) and immobilized on glass fiber (empty dots). 100% TOC at $t = 0$ corresponds to phenol amount before UV irradiation.

The photocatalytic data allow to conclude that the reaction mechanism of immobilized and slurry catalysts is the same and, therefore, the stabilization of the photogenerated electron–hole pairs is the determining step. In particular, in the case of oxidation with H_2O_2 the hindering of the electron–hole recombination is related to the crystal size and shape of particles [23]. Instead, when O_2 is the oxidant, the e^-–h^+ separation depends on the relevant chemisorption of the electron scavenger O_2^- at the surface of catalyst nanoparticles [24].

3.3. Kinetics of PhOH photodegradation in the presence of H_2O_2

In order to obtain deeper insight into the catalytic mechanism of the PhOH photodegradation catalyzed both by TiO_2 coated glass fibers and by powder slurry catalysts, the four parameter kinetic model proposed by Bellobono and co-workers for the partly heterogeneous oxidation, such as that given when operating in the presence of hydrogen peroxide as oxygen donor, was employed [39].

According to this model, it was assumed that the PhOH mineralization to CO_2 occurs through a single intermediate I, which contains the contribution of all intermediates:

$$\mathrm{PhOH} \rightarrow \mathrm{I} \rightarrow \mathrm{CO_2} \tag{13}$$

A system of first order differential equations describes the variation of PhOH, I and CO_2 concentrations [39]:

$$\left(\frac{dC}{dt}\right) = -\frac{k_1 K_1 C}{1 + K_1 C + K_2 C_\mathrm{I}} \tag{14}$$

$$\left(\frac{dC_\mathrm{I}}{dt}\right) = \frac{k_1 K_1 C k_2 K_2 C_\mathrm{I}}{1 + K_1 C + K_2 C_\mathrm{I}} \tag{15}$$

$$\left(\frac{dC_{\mathrm{CO_2}}}{dt}\right) = \frac{k_1 K_1 C_\mathrm{I}}{1 + K_1 C + K_2 C_\mathrm{I}} \tag{16}$$

where C, C_I and C_{co_2} are the concentrations of PhOH, I and CO_2; K_1 and K_2 are the apparent chemisorption constants related to the competitive absorption of, respectively, PhOH and I onto TiO_2 surface; k_1 and k_2 are the kinetic constants of PhOH and I degradation.

When the photodegradation begins, C_I is negligible with respect to C, and the kinetic equations can be approximated to:

$$\left(\frac{dC}{dt}\right) = -\frac{k_1 K_1 C}{1 + K_1 C} \tag{17}$$

At the beginning of the process, when the term $K_1 C > 1$ ($C_{(0)} = 1.53 \times 10^{-3}$ M and the order of magnitude of K_1 reported for PhOH degradation is $\approx 10^7\ \mathrm{M^{-1}}$ [39]), Eq. (17) can be further simplified to a pseudo-zero-order kinetic equation, where $k_{(0)} = k_1$ is the pseudo-zero-order kinetic constant:

$$\left(\frac{dC}{dt}\right) \approx -k_{(0)} \tag{18}$$

Integrating between $t = 0$ and t it results

$$C - C_{(0)} \approx -k_{(0)} t \tag{19}$$

Considering that at the very early stages of reaction the total organic carbon concentration may be assumed $C_\mathrm{TOC} \approx 6$ C, as PhOH contains six carbon atoms, and the very small concentration of intermediates is still given by hydroxylated compounds with the

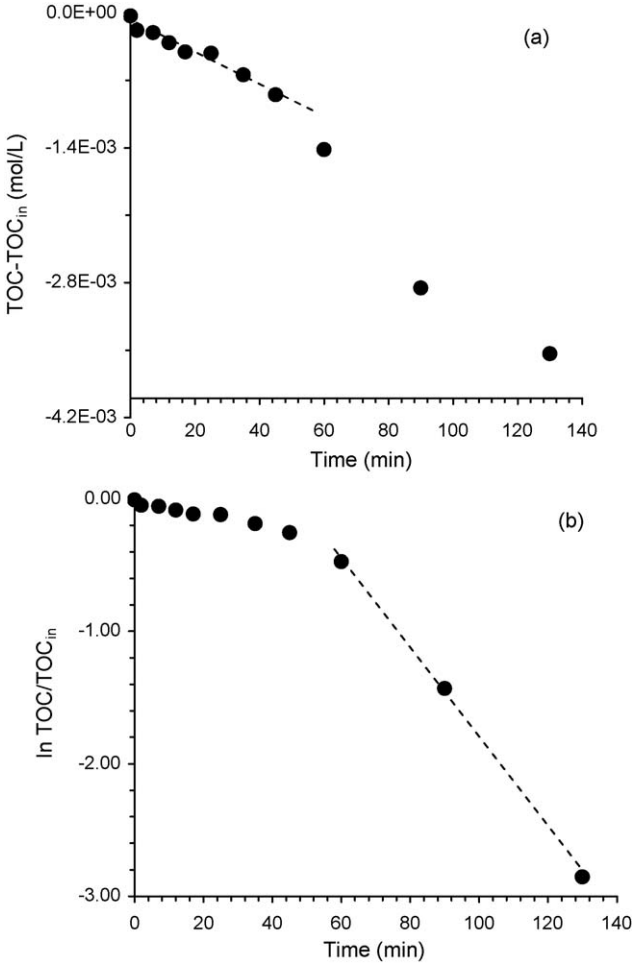

Fig. 5. Plots of (a) (C_{TOC}–$C_{TOC(0)}$) and (b) ln ($C_{TOC}/C_{TOC(0)}$) vs. reaction time calculated from a typical experimental TOC vs. time curve (sample R0 (i)) for the phenol photomineralization in the presence of H_2O_2 as oxygen donor, according to Eqs. (20) and (24).

aromatic ring, Eq. (19) can be written as:

$$C_{TOC} - C_{TOC(0)} \approx -k_{(0)}t \quad (20)$$

by expressing the PhOH concentration in terms of carbon concentration.

On the other hand, at a time t^*, when $C \ll C_I$, the kinetic Eq. (15) can be simplified to:

$$\left(\frac{dC_I}{dt}\right) = -\frac{k_2K_2C_I}{1+K_2C_I} \quad (21)$$

When C_I is very small, Eq. (21) becomes a pseudo-first-order kinetic equation, where $k_{(1)} = k_2K_2$ is the pseudo-first-order kinetic constant:

$$\left(\frac{dC_I}{dt}\right) \approx -k_{(1)}C_I \quad (22)$$

By integrating between t^* and t we obtain:

$$\ln\frac{C_I}{C_{I(t*)}} \approx -k_{(1)}C_I \quad (23)$$

By considering that when $C \ll C_I$, $C_I \approx C_{TOC}$ and that $C_{I(t^*)} \approx C_{TOC(0)}$, Eq. (23) can be rewritten as:

$$\ln\frac{C_{TOC}}{C_{TOC(0)}} \approx -k_{(1)}C_I \quad (24)$$

Table 3
Kinetic constants $k(0)$ and $k(1)$ of TiO_2 coated glass fiber and powder slurry for the photomineralization of phenol in the presence of stoichiometric hydrogen peroxide.

Sample	$k_{(0)}$ (mol min^{-1})	$k_{(1)}$ (min^{-1})
R100	9.40E−05	1.82E−02
R70	8.45E−05	1.82E−02
R57	7.39E−05	1.39E−02
R0	4.21E−05	8.66E−03
P25	6.47E−05	1.26E−02
Blank	8.23E−06	9.37E−03
R100 (i)	1.36E−05	1.39E−02
R70 (i)	1.15E−05	1.28E−02
R57 (i)	1.18E−05	1.26E−02
R0 (i)	8.69E−06	9.90E−03
P25 (i)	9.84E−06	1.12E−02

In Fig. 5(a) and (b) the plots of, respectively (C_{TOC}–$C_{TOC(0)}$) and ln ($C_{TOC}/C_{TOC(0)}$) vs. reaction time, are reported, as calculated for a typical TOC vs. time curve (sample R0 in Fig. 3(a)).

It results that at the beginning of PhOH degradation, the kinetic is of apparent zero order (Fig. 5(a)) while at the end of the process the kinetics approximate a first order reaction. According to Eqs. (19) and (24), $k(0)$ and $k(1)$ can be calculated from the angular coefficients of the straight lines fitting the experimental points.

The values of $k(0)$ and $k(1)$ for all TiO_2 samples, calculated for both TiO_2 coated glass fiber and powder slurry samples from the experimental photodegradation data, are reported in (Table 3).

The fitting of the experimental data by the use of the equations above discussed, demonstrates that the kinetic hypotheses are correctly formulated. Moreover the results show that both $k(0)$ and $k(1)$ values increase with the amount of rutile, their trend resulting parallel to that of $(dC/dt)_{max}$ and $t_{1/2}$ (Table 2). This suggests that the photocatalytic activity of TiO_2, in the presence of hydrogen peroxide as oxygen donor, is depending on the rate of electron–hole recombination both during the initial PhOH photodegradation and during the mineralization of the intermediate compounds.

4. Conclusions

The paper reports on the photoactivity of hydrothermal TiO_2 with different phase compositions, immobilized on glass fiber, used as a catalyst in the PhOH oxidative degradation by H_2O_2 and O_2.

The photocatalytic tests show that immobilized catalysts are active both in partly homogenous (use of H_2O_2 as oxygen donor) and entirely heterogeneous conditions (use of O_2 as oxygen donor). The activity is generally lower for coated glass fibers, if compared with the performances of the same TiO_2 samples in slurries; when the oxidation employs H_2O_2 the reactivity of the immobilized catalyst is comparable (about 1.5 lower) to that of the slurry TiO_2, while it is much lower when the oxygen donor is O_2 (4–5 times).

Nevertheless, the immobilization process does not modify the specific catalytic properties of rutile and anatase, investigated in our previous papers [23,24]. In partly homogeneous phase, being H_2O_2 the oxygen donor, immobilized pure rutile displays the highest catalytic efficiency, in comparison with mixed phase (anatase/rutile) samples and with pure anatase, which show the lowest photocatalytic activity. In entirely heterogeneous phase, being O_2 the oxygen donor, immobilized anatase, both in pure and mixed phase, is essential to improve the photodegradation, while pure rutile displays the lowest catalytic activity.

Analogously to the slurry catalytic experiments, the very high catalytic activity of rutile when H_2O_2 is used, can be explained by the lower tendency of UV generated electrons and holes to recombine in the high crystalline rods of rutile with high aspect ratio when compared to the smaller nanosized particles of anatase (5–15 nm).

Similarly, the higher activity of anatase when the oxygen donor is O_2 can be related to the easy chemisorption of oxygen as O_2^- at the anatase surface [24], acting as an effective electron scavenger. This increases the independent lifetime of electrons and holes, decreasing the electron–hole recombination rate.

The morphology of the hydrothermal TiO_2 nanocrystals observed by electron microscopy explains the different catalytic efficiency of immobilized TiO_2 with respect to powder slurry. The large chestnut burr aggregates of rutile crystalline rods do not form compact aggregates when coated on the glass fiber unlike the small anatase particles do. This maintains a higher free surface area of the supported catalyst, suitable both to UV irradiation and to the adsorption/reaction of PhOH substrate and the oxidative agents. Thus when rutile is the more active species, in the presence of H_2O_2 as catalyst, the reduction of the activity due to immobilization is low and the performance of the coated glass fiber comparable with that of powder slurry. When anatase is the more active species, the relevant particle aggregation decreases the chemisorption of oxygen at the surface and leads to a large decrease of activity.

Acknowledgement

Authors thank the Cariplo Foundation for the financial support.

References

[1] M. Tashibi, C.R. Ngah, N. Aziz, A. Mansor, A.Z. Abdullah, L.K. Teong, A.R. Mohamed, Ind. Eng. Chem. Res. 46 (2007) 9006–9014.
[2] J. Fernandez, J. Kiwi, J. Baeza, J. Freer, C. Lizama, H.D. Mansilla, Appl. Catal. B 48 (2004) 205–211.
[3] J.C. Lee, M.S. Kim, B.W. Kim, Water Res. 36 (2002) 1776–1782.
[4] M.D. Nikolaki, D. Malamis, S.G. Poulopoulos, C.J. Philippopoulos, J. Hazard. Mater. 137 (2006) 1189–1196.
[5] S. Horikoshi, N. Watanabe, H. Onishi, H. Hikada, N. Serpone, Appl. Catal. B 37 (2002) 117–129.
[6] M.K. Aminian, N. Taghavinia, A. Irajizad, S.M. Mahdavi, J. Phys. Chem. C 111 (2007) 9794–9798.
[7] I.N. Martyanov, N.J. Klabunde, J. Catal. 225 (2004) 408–416.
[8] M.G. Antoniou, D.D. Dionysiou, Catal. Today 124 (2007) 215–223.
[9] Y. Xu, C.H. Langford, J. Phys. Chem. B 101 (1997) 3115–3121.
[10] F. Li, S. Sun, Y. Jiang, M. Xia, M. Sun, B. Xue, J. Hazard. Mater. 152 (2008) 1037–1044.
[11] S.N. Hosseini, S.M. Borghei, M. Vossoughi, N. Taghavinia, Appl. Catal. B 74 (2007) 53–62.
[12] S.K. Kansal, M. Singh, D. Sud, J. Hazard. Mater. 153 (2008) 412–417.
[13] T.H. Xie, J. Lin, J. Phys. Chem. C 111 (2007) 9968–9974.
[14] J. Shang, W. Li, Y. Zhu, Mol. Catal. A 202 (2003) 187–195.
[15] N. Kieda, T. Tokuhisa, J. Ceram. Soc. Jpn. 114 (2006) 42–45.
[16] H. Chen, S.W. Lee, T.H. Kim, B.Y. Hur, J. Eur. Ceram. Soc. 26 (2006) 2231–2239.
[17] I.R. Bellobono, R. Barni, F. Gianturco, J. Membr. Sci. 102 (1995) 139–147.
[18] F. Ascari, I.R. Bellobono, P.M. Tozzi, Fresen. Environ. Bull. 12 (2003) 1195–1201.
[19] I.R. Bellobono, F. Ascari, C. Lagrasta, Fresen. Environ. Bull. 12 (2003) 1536–1544.
[20] Z. Liuxue, W. Xiulian, L. Peng, S. Zhixing, Surf. Coat. Technol. 201 (2007) 7607–7614.
[21] B. Tryba, J. Hazard. Mater. 151 (2008) 623–627.
[22] L. Reijnders, J. Hazard. Mater. 152 (2008) 440–445.
[23] A. Testino, I.R. Bellobono, V. Buscaglia, C. Canevali, M. D'Arienzo, S. Polizzi, R. Scotti, F. Morazzoni, J. Am. Chem. Soc. 129 (2007) 3564–3575.
[24] R. Scotti, I.R. Bellobono, C. Canevali, C. Cannas, M. Catti, M. D'Arienzo, A. Musinu, S. Polizzi, M. Sommariva, A. Testino, F. Morazzoni, Chem. Mater. 20 (2008) 4051–4061.
[25] K.S. Mazdiyasni, Ceram. Int. 8 (1982) 42–56.
[26] A. Sclafani, J.M. Herrmann, J. Phys. Chem. 100 (1996) 13655–13661.
[27] P. Salvador, J. Phys. Chem. C 111 (2007) 17038–17043.
[28] U. Diebold, Surf. Sci. Rep. 48 (2003) 53–229.
[29] P. Davit, G. Martra, S. Coluccia, J. Jpn. Petrol. Inst. 47 (2004) 359–376.
[30] J. Theurich, M. Lindner, D.W. Bahnemann, Langmuir 12 (1996) 6368–6376.
[31] R. Vinu, G. Madras, Environ. Sci. Technol. 42 (2008) 913–919.
[32] M. Ampo, T. Shima, Y. Kubokawa, Chem. Lett. 12 (1985) 1799–1801.
[33] K. Okamoto, Y. Yakamoto, H. Tanaka, M. Tanaka, M.A. Itaya, Bull. Chem. Soc. Jpn. 58 (1985) 2015–2016.
[34] E. Selli, I.R. Bellobono, M.L. Raimondi, Angew. Makromol. Chem. 196 (1992) 169–177.
[35] J.H. Baxendale, J.A. Wilson, Trans. Faraday Soc. 53 (1957) 344–355.
[36] T. Ohno, K. Sarukawa, M. Matsumura, New J. Chem. 26 (2002) 1167–1170.
[37] Y. Wang, L. Zhang, K. Deng, X. Chen, Z. Zou, J. Phys. Chem. C 111 (2007) 2709–2714.
[38] K.V. Baiju, S. Shukla, K.S. Sandhya, J. James, K.G.K. Warrier, J. Phys. Chem. C 111 (2007) 7612–7622.
[39] F. Rota, M. Cavassi, D. Niego, R. Gorlani, L. Vianelli, L. Tatti, P. Bruzzi, A. Moroni, I.R. Bellobono, Chemosphere 33 (1996) 2159–2173.